IOPscience iopscience.iop.org

Home Search Collections Journals About Contact us My IOPscience

The effects of back-reaction on turbulence modulation in shear flows: a new exact regularized point-particle method

This article has been downloaded from IOPscience. Please scroll down to see the full text article.

2011 J. Phys.: Conf. Ser. 318 092015

(http://iopscience.iop.org/1742-6596/318/9/092015)

View the table of contents for this issue, or go to the journal homepage for more

Download details:
IP Address: 151.100.85.27
The article was downloaded on 10/01/2012 at 09:58

Please note that terms and conditions apply.

Journal of Physics: Conference Series **318** (2011) 092015 doi:10.1088/1742-6596/318/9/092015

The effects of back-reaction on turbulence modulation in shear flows: a new exact regularized point-particle method

P. Gualtieri, F.Picano, G.Sardina & C.M. Casciola

Dipartimento di Ingegneria Meccanica e Aerospaziale, Via Eudossiana 18, 00184 Roma (ITALY)

E-mail: paolo.gualtieri@uniroma1.it

Abstract. Particles advected by turbulent flows spread non uniformly and form small scale aggregates known as clusters where their local concentration is much higher than it is in nearby rarefaction regions. Recently it has been shown that the addition of a mean flow, through its large scale anisotropy, induces a preferential orientation of the clusters whose directionality can even increase in the smallest scales. Such finding opens new issues in presence of large mass loads, when the momentum exchange between the two phases becomes significant and the back-reaction of the particles on the carrier flow cannot be neglected. These aspects are addressed by direct numerical simulations data of particle laden homogeneous shear flows in the two-way coupling regime. Particles with Stokes number of order one induce an energy depletion of the classical inertial scales and the amplitude increase of the smallest ones where the particle back-reaction pumps energy into the turbulent eddies. We find that increased mass loads results in a broadening of the energy co-spectrum extending the range of scales driven by anisotropic production mechanisms. Such results are obtained in the context of the classical "particle in cell" method. To go beyond this approach we propose a new methodology to model particle laden two phase flows. The method is based on the exact unsteady Stokes solution around a point-particle and is intended to provide a physically consistent picture of the momentum exchange between the carrier and disperse phase.

1. Introduction

Transport of inertial particles is involved in several fields of science such as droplets growth and collisions in clouds, Falkovich *et al.* (2002), the plankton accumulation in the oceans, Lewis & Pedley (2000) or the plume formation in the atmosphere, Woods (2010). Multiphase flows are also fundamental in several technological applications such as the design of internal combustion engines injection systems, Post & Abraham (2002) or the prevention of sediment accumulation in pipelines, Rouson & Eaton (2001).

The relevant physical aspect consists in the particles finite inertia which prevents them from following the fluid trajectories leading to "preferential accumulation". In homogeneous conditions preferential accumulation manifests in the form of small scale clusters where most particles concentrate, see e.g. Bec *et al.* (2007). In inhomogeneous flows, such as wall bounded flows, preferential accumulation occurs in the form of "turbophoresis", i.e. preferential

Published under licence by IOP Publishing Ltd

localization in the near wall region, Reeks (1983); Picano *et al.* (2009), see also Soldati & Marchioli (2009).

The effect of turbulent transport on particle dynamics has been studied extensively. Much less is known about the effect the disperse phase may have on the carrier flow demanding for a renewed effort in this direction see e.g. Balachandar & Eaton (2010); Eaton (2009). It is expected that, under proper coupling conditions, the momentum exchange between the two phases might become relevant in driving the turbulent fluctuations away from their universal equilibrium state predicted by Kolmogorov. Clearly, in contrast to the one-way coupling regime, addressing these effects calls into play the more realistic two-way coupling mechanism, where the disperse phase provides an active modulation of velocity fluctuations.

Important issues such as the increase of the particles settling velocity under gravity have been addressed both numerically, Bosse *et al.* (2006) and experimentally, Yang & Shy (2005). Other effects have been observed in the context of grid generated spatially decaying turbulence where, starting from an isotropic state the particles feed-back leads to an anisotropic flow, Poelma *et al.* (2007). Concerning wall bounded flows new features emerge such as the preferential suppression of turbulence intensities in the wall normal direction, Pan & Banerjee (2001), the enhancement of large scale anisotropy, Yiming *et al.* (2001) or the occurrence of drag reduction Zhao *et al.* (2010). Concerning isotropy when it is broken by gravity or by the mean streamwise advection, the back-reaction seems to immediately originate strong anisotropies in the carrier phase. Motivated by recent findings in the context of anisotropic clustering, Gualtieri *et al.* (2009); Shotorban & Balachandar (2006), we consider the modulation of turbulence in the context of a particle laden homogeneous shear flow where anisotropic effect are disentangled from spatial inhomogeneities.

Modeling the back-reaction in numerical simulations is an issue, der Hoef *et al.* (2008). The local distortion of turbulence can be captured only by resolving the boundary of each particle on the computational grid. In the resolved particle simulations (RPS) several approaches have been proposed ranging from finite volume schemes, Burton & Eaton (2005) to Lattice Boltzman Methods, Poesio *et al.* (2006). Other approaches are possible once it has been recognized that the flow close to a small particle can be locally approximated by the Stokes Flow. In Zhang & Prosperetti (2005), the Stokes solution is used to provide appropriate boundary conditions to the Navier-Stokes equations close to each particle. These approaches, due to their computational cost, are feasible only for a relatively small number of particles. When particles are much smaller than the turbulent scales RPS can not be employed and particles must be considered as material points i.e. as point source/sinks of momentum for the carrier fluid. Within this approximation several other methodologies are available. For instance, the singular steady Stokes solution is employed by Pan & Banerjee (2001) to account for the disturbance flow due to each particle while in the force coupling method, Lomholt & Maxey (2003) the disturbance flow adopts a regularized Stokes solution. The simplest approach is provided by the "particle in cell" method introduced by Crowe *et al.* (1977) which has been widely adopted in the literature.

In this paper we will discuss how, by adopting a proper resolution for the carrier fluid and an by using an appropriate number of particles, the particle in cell method is still able to capture meaningful turbulence modification effects. After discussing its limitations we will present a new approach to model the momentum coupling between the two phases. The new methodology is based on the exact unsteady Stokes solution around a point-particle as will be reported in detail in this contribution.

2. Point-particles: review and results

The carrier fluid flow is a homogeneous shear flow. The velocity field $\mathbf{v}$ is decomposed into a mean flow $\mathbf{U} = Sx_2\,\mathbf{e}_1$ and a fluctuation $\mathbf{u}$ where $\mathbf{e}_1$ is the unit vector in the streamwise direction, x_2 denote the coordinate in the direction of the mean shear S and x_3 is in the spanwise

direction. Rogallo's technique, Rogallo (1981) is employed to write the Navier-Stokes equations for velocity fluctuations in a deforming coordinate system convected by the mean flow according to the transformation of variables $\xi_1 = x_1 - Stx_2; \quad \xi_2 = x_2; \quad \xi_3 = x_3; \quad \tau = t$. The resulting system

$$\nabla \cdot \mathbf{u} = 0\,; \qquad \frac{\partial \mathbf{u}}{\partial \tau} = (\mathbf{u} \times \boldsymbol{\zeta}) - \nabla \pi + \nu \nabla^2 \mathbf{u} - S u_2 \mathbf{e}_1 + \mathbf{F}\,, \tag{1}$$

is numerically integrated by a pseudo-spectral method combined with a fourth order Runge-Kutta scheme for temporal evolution. In equations (1) $\boldsymbol{\zeta}$ is the curl of $\mathbf{u}$, π is the modified pressure which includes the fluctuating kinetic energy $|\mathbf{u}|^2/2$, ν is the kinematic viscosity and $\mathbf{F}$ denote the back-reaction due to the disperse phase. The latter consists of diluted particles with mass density ρ_p much larger than the carrier fluid ρ_f. The approximation of point particles can be adopted whenever the particle diameter d_p is much smaller than the typical turbulence scales. It follows that the only relevant force is the Stokes drag Maxey & Riley (1983). Accordingly, the equations for particles position $x_i^p(t)$ and velocity $v_i^p(t)$ are $\dot{x}_i^p = v_i^p\,; \quad \dot{v}_i^p = f_i^p$ where $v_i(x^p, t)$ is the instantaneous fluid velocity evaluated at $x_i^p(t)$, $f_i^p = \tau_p^{-1}\left[v_i(x^p, t) - v_i^p(t)\right]$ is the Stokes drag, $\tau_p = \rho_p d_p^2/(18\nu\rho_f)$ is the Stokes relaxation time and the dot denote time derivative. According to the particle in cell method the back-reaction on the fluid is computed as $\mathbf{F} = -\left(N_c/N_p\right)\Phi \sum_p^{n(\xi)} \mathbf{f}^p$ where the sum is extended to all the $n(\xi)$ particles belonging to the computational cell centered at point ξ. N_c denote the number of Eulerian cells, N_p is the total number of particles and Φ denote the mass load ratio i.e. the ratio between the mass of the disperse phase $M_p = N_p \pi \rho_p d_p^3/6$ and the carrier fluid $M_f = \rho_f V_f$ where V_f is the volume of the computational box. Since fluid properties are known in an Eulerian frame a first interpolation of the fluid velocity at the particle position is required to evaluate the Stokes drag. A second interpolation is used when the back-reaction on the fluid is computed. Actually, the force f_i^p acting on the p^{th} particle is re-distributed via inverse interpolation to the nearest Eulerian grid points. In our case we adopted a tri-linear scheme.

Concerning the homogeneous shear flow, the mean shear induces velocity fluctuations which are anisotropic at the larger scales driven by production while, at smaller separations, the classical energy transfer mechanisms become effective in inducing re-isotropization. The transition between the two regimes occurs across the shear scale $L_S = \sqrt{\epsilon/S^3}$. The dynamics of the disperse phase is controlled by the Stokes number $St_\eta = \tau_p/\tau_\eta$ ratio of the particles relaxation time τ_p to a characteristic flow time scale, typically the Kolmogorov time scale $\tau_\eta = (\nu/\epsilon)^{1/2}$.

In the two-way coupling regime, the mass load fraction $\Phi = M_p/M_f$, is required as additional dimensionless parameter to describe the momentum exchange between the two phases. We will address data at a Taylor Reynolds number of $Re_\lambda = 50$ corresponding to a Kolmogorov scale $\eta = 0.07$ with a shear parameter $S^* = (L_0/L_S)^{2/3} = 7$ advecting particles with unitary Stokes number. The grid resolution, the total number of particles and the mass load ratio will be varied to address different numerical and physical issues.

A detailed analysis of turbulence modulation calls into play the spectral distribution of the turbulent kinetic energy. In figure (1) we show the energy spectra for the data at $\Phi = 0.4$ with an Eulerian resolution of $384 \times 192 \times 192$ Fourier modes. By systematically changing the number of particles per cell, namely N_p/N_c, we observe how turbulent fluctuations are first attenuated in an intermediate range of scales to be eventually enhanced at the smallest ones. However, besides this general result, we observe a different behavior of the energy distribution at the smallest scales depending of the ratio N_p/N_c. For instance, as we diminish N_p/N_c the smallest scale seems to be more energized with respect to a case where more particles per cell are available. This is due to the back reaction field which, being spatially localized at the particle position, becomes progressively more spotty and intermittent when the Stokes drag is interpolated into the Eulerian grid. The same comments hold for the energy cospectrum shown in the inset of figure (1) (left panel) and for the dissipation spectrum plotted in the right panel of the same

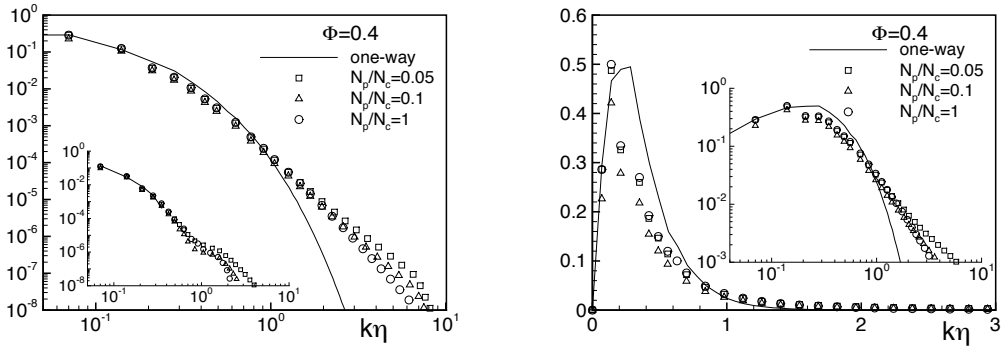

Figure 1. Effect of the number of particles per cell N_p/N_c on the energy spectra at $\Phi = 0.4$ and fixed grid resolution of $384 \times 192 \times 192$ Fourier modes. Left: energy spectrum and cospectrum (inset). Right: dissipation spectrum in linear scale, in the inset the same data are plotted in logarithmic scale.

figure. The effect of the number of particles per cell N_p/N_c can be better appreciated when data are plotted in a logarithmic scale. When the data are represented in linear scale to better evaluate the area below the curve–its integral amounts for the total viscous energy dissipation rate–the effect of N_p/N_c is hardly appreciated. Such result allows to exclude any bias due to the injection of the back-reaction field into the Eulerian grid which might effect the results if it operates in a range of physically meaningful scales. Under this respect, the most critical quantity is the energy dissipation rate. Indeed, even this quantity is not affected if a proper resolution is adopted i.e. if enough scale separation between the physically active scales and the scales of the order of the grid size is allowed. However, this is a strong resolution requirement which compels the use of a fine grid even at a relatively small Reynolds number.

To complete the analysis of the point-particle method in figure (2) we explore the convergence of the solution on different Eulerian grids when the mass load ratio Φ and the number of particles per cell N_p/N_c are fixed. In figure (2) we compare energy spectrum (left panel) and cospectrum (right panel) for three different data sets. For instance, we fixed the mass load ratio $\Phi = 0.4$ and considered two values of the mean particle concentration. For $N_p/N_c = 1$ we refined the Eulerian grid from $192 \times 96 \times 96$ to $384 \times 192 \times 192$ Fourier modes while for $N_p/N_c = 7$ we refined the grid from $96 \times 48 \times 48$ to $192 \times 96 \times 96$ Fourier modes. Good convergence of the energy spectra is observed in the scale range common to both data sets. In the inset similar data for $\Phi = 0.8$ and $N_p/N_c = 7$ show the same behavior. The analysis also allows to establish the minimum number of particles per cell required to achieve a convergence see e.g. the two data sets with the same grid resolution $192 \times 96 \times 96$ Fourier modes, the same mass load $\Phi = 0.4$, but different values of N_p/N_c. When the number of particles per cell is varied from one to seven, the spectra seem to be unaffected in the whole range of resolved scales.

From the above analysis we might draw some conclusions. The back reaction field becomes progressively more spotty and intermittent as the Eulerian grid is refined. This effect might be compensated by increasing the mean number of particle per cell. Secondly, since the back-reaction field is grid-dependent, a sufficient separation between the physically active scales and the grid size is needed. This constraint strongly limits the Reynolds number that can be simulated with a given Eulerian grid. Such drawbacks are essentially due to the numerical implementation of the coupling mechanism which simply redistributes the force acting on a particle to the computational cell the particle belongs to. In fact, the regularization of the back-reaction field is provided by the interpolation scheme and by the implicit filter represented

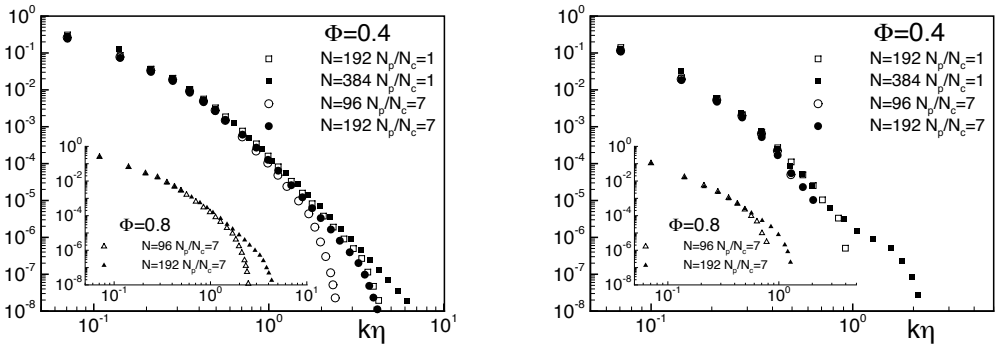

Figure 2. Effect of the Eulerian grid resolution on the energy spectra. A coarse grid (open symbols) is compared against a finer one (filled symbols) for a given value of the particles per cell ratio N_p/N_c and mass load Φ. Left: energy spectrum at $\Phi = 0.4$, the squares refer to $N_p/N_c = 1$ for two Eulerian resolutions, namely $192 \times 96 \times 96$ (open squares) and $384 \times 192 \times 192$ (filled squares). The circles correspond to $N_p/N_c = 7$ for a coarse $96 \times 48 \times 48$ (open circles) and finer $192 \times 96 \times 96$ (filled circles) grid respectively. In the inset analogous data at $\Phi = 0.8$ and $N_p/N_c = 7$, for the coarse $96 \times 48 \times 48$ and the finer $192 \times 96 \times 96$ grid respectively. Right: same data as in the left panel concerning the energy copectrum.

by the Eulerian grid.

3. Exact Regularized Point Particle (ERPP) method: overview and results

Motivated by the results discussed in the previous section we present here a new coupling method to account for the momentum exchange between the carrier and the disperse phase.

A point particle of mass m_p in the relative motion with respect to a Newtonian fluid experiences a drag force which can be modeled in terms of the Stokes drag $\mathbf{D}(t) = 3\pi\mu d_p \{\tilde{\mathbf{u}}[\mathbf{x}_p(t), t] - \mathbf{v}_p(t)\}$ where μ is the dynamic viscosity of the fluid, d_p is the diameter of the particle, here assumed to be spherical. The expression of the Stokes drag involves the fluid velocity evaluated away from the particle i.e. in the particle scale, the fluid velocity at infinity. This is an issue when two-way coupling is addressed since each particle produces a self-disturbance flow. We use the Faxen correction to estimate the far field fluid velocity $\tilde{\mathbf{u}}(\mathbf{x}_p, t) = \mathbf{u}(\mathbf{x}_p, t) + L_\infty^2/24\nabla^2\mathbf{u}(\mathbf{x}_p, t)$ where the regularization scale L_∞ is set by matching the terminal particle velocity in still fluid.

In an Eulerian framework the force on the point particle is a singular field $\mathbf{F}(\mathbf{x}, t) = -\mathbf{D}(t)\,\delta[\mathbf{x} - \mathbf{x}_p(t)]$ where $\mathbf{F}(\mathbf{x}, t)$ is the force the particle exerts back on the carrier fluid and $\delta(\mathbf{x})$ is the Dirac delta function. In such conditions, on a scale much larger than the particle size but still much smaller than the relevant spatial scales of the carrier flow, the fluid motion is well described by the incompressible Stokes equations,

$$\frac{\partial \mathbf{v}}{\partial t} - \nu\nabla^2\mathbf{v} + \nabla p = \mathbf{F}, \quad \mathbf{v}(\mathbf{x}, 0) = \mathbf{v}_0(\mathbf{x}) \tag{2}$$

where $\mathbf{v}_0$ is the velocity field assigned as initial condition. Peculiarity of the mathematical model we are using is that the linear, unsteady part of the fluid acceleration term has been retained in eq. (2), even though it could have been neglected on the basis of the typical time scale of the phenomenology. As we shall see, this choice will allow a well defined procedure to regularize the solution of the coupled flow problem, where the particle reacts back on the fluid.

Our problem consists in determining an efficient algorithm for a consistent and accurate approximation of the solution of the singularly forced Stokes equation (2) able to allow the coupling of the intermediate scale problem with the large scale, high Reynolds number solution of the fully non-linear Navier-Stokes equation.

The algorithm we devise exploits the localization operated by the diffusion equation for the intermediate scale vorticity field associated to the particle motion $\boldsymbol{\zeta}(\mathbf{x},t) = \nabla \times \mathbf{v}(\mathbf{x},t)$,

$$\frac{\partial \boldsymbol{\zeta}}{\partial t} - \nu \nabla^2 \boldsymbol{\zeta} = \nabla \times \mathbf{F} = \mathbf{D}(t) \times \nabla \delta \left[\mathbf{x} - \mathbf{x}_p(t)\right], \quad \boldsymbol{\zeta}(\mathbf{x},0) = \boldsymbol{\zeta}_0(\mathbf{x}). \tag{3}$$

The above linear problem can be split in a forced problem with homogeneous initial conditions and the free diffusion of the initial vorticity with non homogeneous initial conditions $\boldsymbol{\zeta} = \boldsymbol{\zeta}^f + \boldsymbol{\zeta}^h$. The solution is explicitly expressed as a convolution with the fundamental solution of the diffusion equation, $\partial_t g - \nu \nabla^2 g = \delta(\mathbf{x} - \xi)\,\delta(t - \tau)$ given by $g(\mathbf{x},\xi,t,\tau) = \exp\left\{-|\mathbf{x}-\xi|^2/\left[4\nu(t-\tau)\right]\right\}/\left[4\pi\nu(t-\tau)\right]^{3/2}$ which corresponds to a Gaussian with time dependent variance $\sigma(t-\tau) = \sqrt{2\nu(t-\tau)}$.

The solution of the forced problem with homogeneous initial conditions is given by

$$\boldsymbol{\zeta}^f(\mathbf{x},t) = \int_0^t \mathbf{D}(\tau) \times \nabla g\left[\mathbf{x} - \mathbf{x}_p(\tau), t - \tau\right] d\tau\,, \tag{4}$$

while the solution of the homogeneous equation is given by the standard spatial convolution with the fundamental solution,

$$\boldsymbol{\zeta}^h(\mathbf{x},t) = \int \boldsymbol{\zeta}_0(\xi,t) g(\mathbf{x},\xi,t,0) d\xi. \tag{5}$$

The vorticity field is apparently singular. The singularity comes from the contribution to the integral near the upper integration limit, $\tau \simeq t$, where $g(\mathbf{x},\xi,t,\tau)$ tends to behave as badly as the Dirac delta function. On the contrary, due to the strong regularization operated by the diffusion operator, away from the upper integration limit the integrand is smooth. We can then define a regularization procedure based on a temporal cut-off ϵ such that the vorticity is additively split into a regular and a singular component, $\boldsymbol{\zeta}^f(\mathbf{x},t) = \boldsymbol{\zeta}_R(\mathbf{x},t,\epsilon) + \boldsymbol{\zeta}_S(\mathbf{x},t,\epsilon)$ with smooth and singular part respectively given by

$$\boldsymbol{\zeta}_R(\mathbf{x},t) = \int_0^{t-\epsilon} \mathbf{D}(\tau) \times \nabla g\left[\mathbf{x} - \mathbf{x}_p(\tau), t - \tau\right] d\tau\,, \tag{6}$$

and by

$$\boldsymbol{\zeta}_S(\mathbf{x},t) = \int_{t-\epsilon}^{t} \mathbf{D}(\tau) \times \nabla g\left[\mathbf{x} - \mathbf{x}_p(\tau), t - \tau\right] d\tau\,. \tag{7}$$

The regular field $\boldsymbol{\zeta}_R$ can be interpreted as the free diffusion in the time interval $[t-\epsilon, t]$ of the complete field, superposition of regular and singular components, at time $t-\epsilon$, $\boldsymbol{\zeta}^f(\mathbf{x}, t-\epsilon)$,

$$\boldsymbol{\zeta}_R(\mathbf{x},t) = \int \boldsymbol{\zeta}^f(\boldsymbol{\xi}, t-\epsilon) g\left[\mathbf{x} - \boldsymbol{\xi}, \epsilon\right] d\boldsymbol{\xi}\,, \tag{8}$$

where the spatial convolution of the field $\boldsymbol{\zeta}^f$ at time $t-\epsilon$ with the fundamental solution of the diffusion equation with time argument ϵ propagates forward the field from $t-\epsilon$ to time t. The regular part of the vorticity field, $\boldsymbol{\zeta}_R$, is everywhere smooth and characterized by the smallest

spatial scale $\sigma(\epsilon) = \sqrt{2\nu\epsilon}$. It is easy to derive the differential equation satisfied by $\boldsymbol{\zeta}_R(\mathbf{x}, t)$ namely

$$\frac{\partial \boldsymbol{\zeta}_R}{\partial t} - \nu\nabla^2\boldsymbol{\zeta}_R = -\nabla_x \times \mathbf{D}(t-\epsilon)g\left[\mathbf{x} - \mathbf{x}_p(t-\epsilon), \epsilon\right] , \quad t > \epsilon; \quad \boldsymbol{\zeta}_R(\mathbf{x}, \epsilon) = 0 . \tag{9}$$

The decomposition of the vorticity field into smooth and singular components can be exploited in an efficient computational algorithm to couple the dynamics of the two phases. Given its smoothness properties the field $\boldsymbol{\zeta}_R(\mathbf{x}, t)$ can be represented on a discrete grid, provided the grid size Δ is comparable with the smallest scale of the field $\sigma(\epsilon)$. In fact, the vorticity field given by eq.(9) provides the regularized disturbance produced by a small spherical particle experiencing the drag force $\mathbf{D}(t)$. By standard techniques the disturbance vorticity can be rec into a corresponding disturbance velocity field which is then injected into the Eulerian grid.

In order to evaluate the proposed method we consider the unsteady motion of a single spherical particle settling from rest under the effect of a constant body force e.g. gravity which is then removed at latter times. The problem is challenging. Actually, when considering only a single particle in the two-way coupling regime the only modification of the flow is induced by the particle itself. This requires an accurate evaluation of the Stokes drag by means of the Faxen correction discussed above. Moreover, the motion of the particle is unsteady as it would be in a real turbulent flows where the particle experiences continuos variation of the fluid motion along its trajectory. The velocity of the particle resulting from the ERPP calculations are shown in figure (3). The data are compared with a spatially resolved numerical simulation around a finite size particle obtained by the *Comsol Multiphysics* solver. The ERPP results are shown for different values of the regularizing parameter $\sigma(\epsilon)$ and present good agreement with the resolved simulation data. Note that both the transient motion and the terminal velocity are correctly estimated by the ERPP method. In the inset, we have checked the sensitivity of the ERPP to the particle Reynolds number.

Second and more severe check is provided in figure (4) where we plot the disturbance velocity

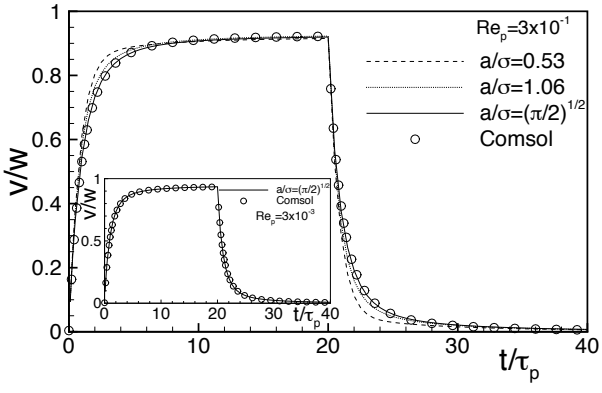

Figure 3. Particle velocity versus time: the particle is accelerated from rest at $t = 0$ by means of a constant external force. Successively at $t/\tau_p = 20$ the force is removed and the particle is progressively decelerated by the Stokes drag. The particle velocity is normalized by the Stokes settling velocity $w = \tau_p f$ where f is the external force. Time is rescaled by the Stokes time τ_p. Data corresponds to a particle Reynolds number $Re_p = w\, d_p/\nu = 3 \cdot 10^{-1}$. In the inset same data at $Re_p = 3 \cdot 10^{-3}$. The lines correspond to different values of the ratio $a/\sigma(\epsilon)$ where a is the particle radius, the open symbols are the data provided by *Comsol Multiphysics*.

profiles computed by the ERPP in comparison with the *Comsol Multiphysics* solution. We present the velocity along the settling direction (left column) and along the transversal direction (right column). Panels from top to bottom refer to different times across the particle trajectory. At all times the ERPP solution is able to capture the spatial structure of the disturbance flow as compared to the fully resolved numerical data. In the plot we have reported the corresponding steady Stokes and Oseen-improved solution past a sphere. Note that the quasi-steady approximation for the disturbance field is quite inaccurate especially at early times when the particle accelerates from rest. This is crucial in turbulence when the particle evolves subject to the sudden acceleration induced by the chaotic nature of the flow. On the contrary, the present solution fully captures such unsteadiness. The ERPP method is also able to capture the flow front-back symmetry breaking due to finite Reynolds number effects along the transient phase. Actually at steady state the solution is better described by the Oseen solution rather than

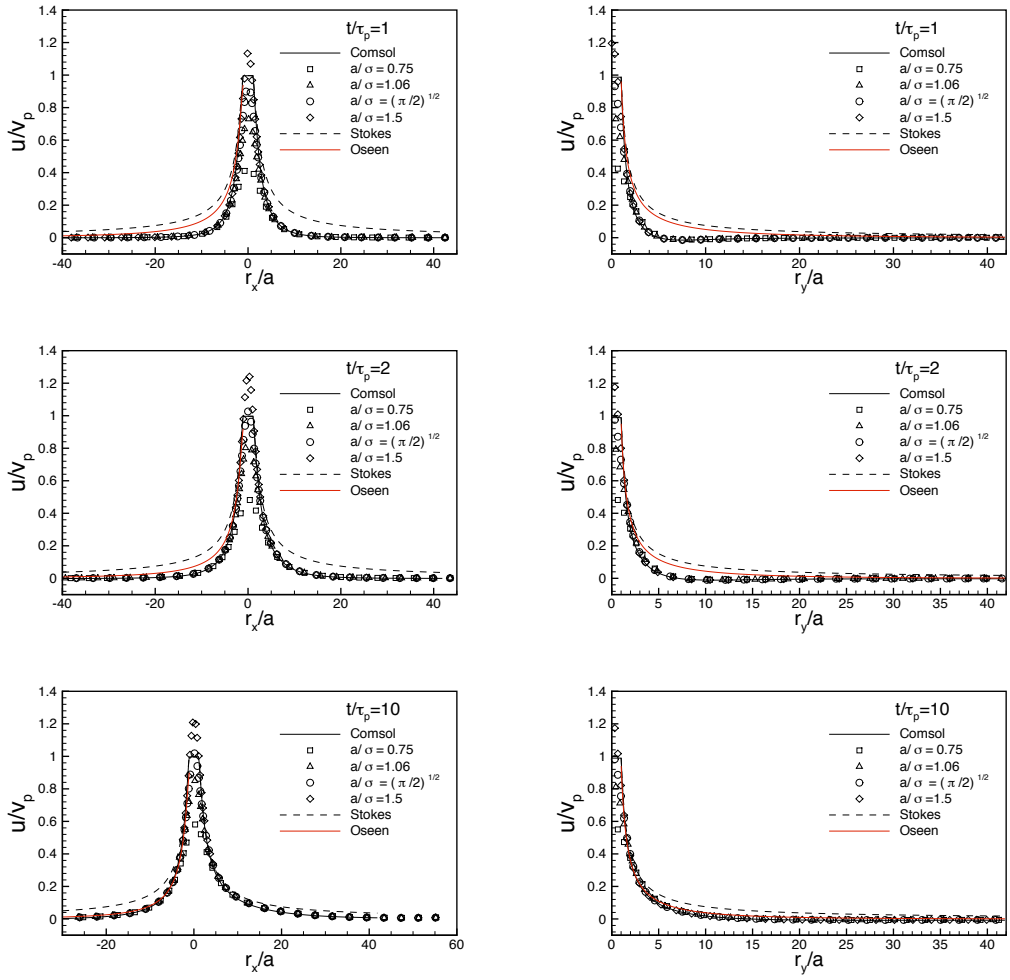

Figure 4. Flow disturbance due to a particle moving from left to right. 1D profiles of the streamwise velocity in the parallel (left) and transversal (right) directions. Panels from top to bottom correspond to different times namely $t/\tau_p = 1, 2, 10$. The ERPP results for different values of a/σ (symbols) are compared against the solution provided by *Comsol Multiphysics* (solid line). For comparison we provide the steady Stokes solution (dashed line) and the Oseen-improved correction (red solid line).

the Stokes solution. As a final comment, we observe that the finest details close to the particle boundary are sensitive to the ratio a/σ. In particular, as already addressed by Lomholt & Maxey (2003) for the steady Stokes solution, for $a/\sigma = (\pi/2)^{1/2}$ the disturbance flow reproduces the rigid motion of the sphere by matching the rigid body velocity at the center. We find that this result holds also during the transient phase at least for $t \geq \tau_p$. However, irrespective of the value of a/σ, the far field behavior does not change. For instance, the ERPP solution collapse on the *Comsol Multiphisics* solution already after a few particle's radius. This is extremely important since our aim consist in the simulation of a large ensemble of point-particles where it is unfeasible to resolve the spatial scales comparable with the particle radius.

4. Final remarks

We have discussed DNS data of a particle laden homogeneous shear flow in the two-way coupling regime. Concerning the alteration of turbulence we found that particles with Stokes number of order one induce an energy depletion of the classical inertial scales and the amplitude increase of the smallest ones where the particle back-reaction pumps energy into the turbulent eddies. We also find a broadening of the energy co-spectrum extending the range of scales driven by anisotropic production mechanisms. As far as the "particle in cell" method is correct our results are physically meaningful. In fact, as the particle in cell back-reaction field is grid-dependent, we took care to have a sufficient separation between the physically active scales and the grid size before drawing our physical conclusions. To overcome the limitations of the method we have developed a new approach to account for the momentum exchange between the two phases. The new methodology, based on the exact unsteady Stokes solution around a point-particle, has been tested in the simple case of a point particle settling under gravity. The method provides a physically consistent picture of the momentum coupling between the carrier and disperse phase. In fact, the ERPP is able to reproduce both the particle transient motion and the finest spatial details of the induced disturbance flow. The ERPP is expected to provide accurate and efficient results for turbulent particle-laden flows, when the particle size is sufficiently smaller than the typical Kolmogorov scale of the flow.

References

Balachandar, S. & Eaton, J.K. 2010 Turbulent dispersed multiphase flow. *Ann. Rev. Fluid Mech* **42**, 111–133.

Bec, J., Biferale, L., Cencini, M., Lanotte, A., Musacchio, S. & Toschi, F. 2007 Heavy particle concentration in turbulence at dissipative and inertial scales. *Phys. Rev. Lett.* **98(8)**, 084502.

Bosse, T., Kleiser, L. & Meiburg, E. 2006 Small particles in homogeneous turbulence: settling velocity enhancement by two way coupling. *Phys. Fluids* **18**, 0271021.

Burton, T.M. & Eaton, J.K. 2005 Fully resolved simulations of a particle-turbulence interaction. *J. Fluid Mech.* **545**, 67–111.

Crowe, C.T., Sharma, M.P. & Stock, D.E. 1977 The particle source in cell (psi-cell) model for gas-droplet flows. *J. Fluid Eng.* **99(2)**, 325.

Eaton, J.K. 2009 Two-way coupled turbulence simulations of gas-particle flows using point-particle tracking. *Int. J. Multiphase flow* **35(9)**, 792–800.

Falkovich, G., Fouxon, A. & Stepanov, M. 2002 Acceleration of rain initiation by cloud turbulence. *Nature* **419**, 151.

Gualtieri, P., Picano, F. & Casciola, C.M. 2009 Anisotropic clustering of inertial particles in homogeneous shear flow. *J. Fluid Mech.* **629**, 25–39.

der Hoef, M.A. Van, Annald, M. Van Sint, Deen, N.G. & Kuipers, J.A.M. 2008 Numerical simulations of dense gas-solid fluidized beds: a multiscale modeling strategy. *Ann. Rev. Fluid Mech* **40**, 47–70.

Lewis, D. & Pedley, T. 2000 Plantonik contact rates in homogeneous isotropic turbulence: theoretical predictions and kinematic simulations. *J. Thoretical Biology* **205**, 377–408.

Lomholt, S. & Maxey, M.R. 2003 Force-coupling method for particulate two phase flow: Stokes flow. *J. Comp. Phys.* **184**, 381–405.

Maxey, M.R. & Riley, J.J. 1983 Equation of motion for a small rigid sphere in a nonuniform flow. *Phys. Fluids* **26**, 2437.

Pan, Y. & Banerjee, S. 2001 Numerical simulation of particle interaction with wall turbulence. *Phys. Fluids* **8(10)**, 2733–2755.

Picano, F., Sardina, G. & Casciola, C.M. 2009 Spatial development of particle-laden turbulent pipe flow. *Phys. Fluids* **21**, 093305.

Poelma, C., Westerweel, J. & Ooms, G. 2007 Particle-fluid interaction in grid generated turbulence. *J. Fluid. Mech.* **589**, 315.

Poesio, P., Ooms, G., Cate, A. Ten & Hunt, J.C.R. 2006 Interaction and collisions between particles in a linear shear flow near a wall at low reynolds number. *J. Fluid Mech.* **555**, 113–130.

Post, S.L. & Abraham, J. 2002 Modeling the outcome of drop-drop collisions in diesel sprays. *Int. Journal Mult. Flows* **28** (6), 997–1019.

Reeks, M.W. 1983 The transport of discrete particles in inhomogeneous turbulence. *J. Aerosol Sci.* **14** (6), 729–739.

Rogallo, R.S. 1981 Numerical experiments in homogeneous turbulence. *Nasa T-M* **81315**.

Rouson, D.W. & Eaton, J.K. 2001 On the preferential concentration of solid particles in turbulent channel flow. *J. Fluid Mech.* **428**, 149.

Shotorban, B. & Balachandar, S. 2006 Particle concentration in homogeneous shear turbulence simulated via lagrangian and equilibrium eulerian approaches. *Phys. Fluids.* **18**, 065105.

Soldati, A. & Marchioli, C. 2009 Physics and modelling of turbulent particle deposition and entrainment: review of a systematic study. *Int. J. Multiphase flow* **35(9)**, 827–839.

Woods, W. A. 2010 Turbulent plumes in nature. *Ann. Rev. Fluid Mech* **42**, 391–412.

Yang, T.S. & Shy, S.S. 2005 Two-way interaction between solid particles and homogeneous air turbulence: particle settling rate and turbulence modulation measurements. *J. Fluid Mech.* **526**, 171–216.

Yiming, L., McLaughlin, J.B., Kontomaris, K. & Portela, L. 2001 Numerical simulation of particle-laden turbulent channel flow. *Phys. Fluids* **13(10)**, 2957–2967.

Zhang, Z. & Prosperetti, A. 2005 A second order method for three dimensional particle simulation. *J. Comp. Phys.* **210**, 292–324.

Zhao, L.H., Andersson, H.I. & Gillisen, J.J. 2010 Turbulence modulation and drag reduction by spherical particles. *Phys. Fluids* **22**, 0817021.